

No Evidence for Room Temperature Ferromagnetism in the High Temperature Metal-Organic Material: Ni_2TCNQ

Adam Berlie

ISIS Neutron and Muon Source, STFC Rutherford Appleton Laboratory, Chilton, Oxfordshire, OX11 0QX, United Kingdom
Department of Physics, Durham University, South Road, Durham, DH1 3LE, United Kingdom.

E-mail: adam.berlie@stfc.ac.uk

Ian Terry

Department of Physics, Durham University, South Road, Durham, DH1 3LE, United Kingdom.

Marek Szablewski

Department of Physics, Durham University, South Road, Durham, DH1 3LE, United Kingdom.

Kimberly Quinn

Department of Physics, Durham University, South Road, Durham, DH1 3LE, United Kingdom.

Abstract. The search for ferromagnetic organic-based compounds has been a particular challenge to both chemists and physicists over the past few decades. The synthesis of the Ni_2A , where A is an organic acceptor; TCNE, DDQ or TCNQ [*Nature* **445**, 291], was reported to be a great advancement with claims that the ferromagnetism persisted to well above room temperature. There were, however some substantial flaws in the methodology associated with the synthesis and physical characterisation. Our work solely studies the Ni_2TCNQ compound where we find no evidence for the existence of inherent ferromagnetism within the material that was reported in the original paper. Instead, we find that the magnetism is due to superparamagnetic nickel nanoparticles embedded in an amorphous matrix. It is hoped that our work will also show that one must be careful when using $\text{Ni}(\text{COD})_2$ as a precursor in the synthesis of magnetic materials and that the usefulness of the reported synthetic method is extremely limited.

1. Introduction

There are many advantages to working with organic based materials; they provide us with a cheap synthetic route when compared to their inorganic counterparts, their

properties can be tuned through the use of bottom-up chemistry and there is potential for them to show plastic or flexible properties. One area where organic based materials have found a lot of interest is in magnetism where these “synthetic magnets” have shown promise as new types of compounds that could replace some inorganic or oxide magnets within devices [1, 2]. One of the first and most prominent examples of this was the discovery of vanadium bis-tetracyanoethene, that shows magnetic order at room temperature with a transition temperature of approximately 400 K [3]. However, the sample shows no long range structural order and so the magnetism is thought to correlate through a percolative mechanism. Nevertheless, the magnetism remained extremely sensitive to both the synthetic route and organic acceptor being used illustrating its promise as a truly tuneable system [4, 5, 6, 7]. Another area of work that has attracted a large amount of attention is that by Jain *et al.* where they reported novel magnetic samples with the formula Ni_2A , where A is an organic acceptor of either 3-dichloro-5,6-dicyano-1,4-benzoquinone (DDQ), tetracyanoethene (TCNE) or 7,7,8,8-tetracyanoquinodimethane (TCNQ) [8]. The reactions involved mixing a zero-valent form of Ni (in $Ni(COD)_2$) with the organic acceptor in dichloromethane (DCM) initially under an inert atmosphere and then exposing the reaction mixture to air. This resulted in a black powder that at room temperature is attracted to a magnet if held close by and showed a distinct magnetic response under closer investigation. Questions do arise from this work as all samples were amorphous yet exhibited an apparently strong magnetic response; thus the materials warranted further investigation. Miller and Pokhodnya substituted DCM in the reaction for tetrahydrofuran (THF) and reported the synthesis of a black powder that they claimed was $Ni(TCNE)_2 \cdot 3.45(THF)$ [9]. This compound showed a downturn at 15 K in the χT vs. T data, where temperatures above this, the inverse magnetic susceptibility is believed to be linear once a background from 300 ppm of Ni(0) had been subtracted. This prompted some concern about the origins of the magnetism within the Ni_2A salts and highlighted ambiguities within the original work by Jain *et al.* [8]. In fact earlier work on the stoichiometric compound of $Ni(TCNQ)_2$ was reported by Cl erac *et al.* [10] where subsequent measurements have confirmed the presence of a ferromagnetic state only below 20 K [11, 12].

Previous work by us on nominal Ni_2A salts showed that, when swapping the TCNQ for tetrafluoro-TCNQ ($TCNQF_4$), a black powder was formed with similar magnetic properties to that observed within Ni_2TCNQ [13]. However, the magnetic properties showed a solvent dependency and when a nitrile-based solvent was used, this caused there to be a significant change in the room temperature magnetism. From microscopy work, we were able to show that the resultant magnetism was from larger nickel particles present within the sample. When using a nitrile-based solvent, this stabilised nickel clusters and in fact these clusters can also be observed simply from the slow decomposition of nickel bis-1,5-cyclooctadiene ($Ni(COD)_2$) [14].

This paper presents results from our replication of the Ni_2TCNQ work previously reported by Jain *et al.* [8]. Firstly we report results from a direct comparison with the Ni_2TCNQ synthesis where we show that the resulting magnetism is due, not to a

metal-organic phase, but to the presence of nickel nanoparticles where there is no bulk ferromagnetic transition between 200 and 460 K, above which the sample begins to decompose. Secondly we show that by using tetrahydrofuran (THF) as the solvent within the synthetic route we are able to suppress the large agglomeration of Ni nanoparticles and instead stabilise small Ni clusters.

2. Experimental

Samples of Ni_2TCNQ were synthesised using the same method as reported by Jain *et al.* [8]. We used a 2:1 ratio of $Ni(COD)_2$ (0.38 g) to TCNQ (0.13 g), where the TCNQ was first dissolved in 70 cm³ of anhydrous dichloromethane to form a translucent, yellow solution. The $Ni(COD)_2$ was then dissolved in 30 cm³ of anhydrous dichloromethane that formed a dark yellow solution. All solutions were made under an argon atmosphere. On mixing, the colour of the solution changed from yellow to cloudy and dark green, indicating the some of the TCNQ was being reduced. The solution was stirred under argon for three hours and then exposed to air using a septum and needle to allow a slow mixing of the air. This was then left to stir for two hours where a black powder formed, which could be filtered and washed with dichloromethane. The resulting dry powder was black with a slight blue tinge. An additional sample was made using the same synthetic route where the dichloromethane was replaced with tetrahydrofuran. The yield is particularly low and varies hugely indicating that a lot of the TCNQ or Ni is lost within the solvent when the solid is filtered off. Elemental analysis and inductively-coupled plasma mass spectroscopy was used to gain the atomic percentage weights of Ni_2TCNQ sample. The found % weight values are: C 35.91, H 2.43, N 12.20 and Ni 33.79. Using the ratio of Ni:N as a marker for the stoichiometry of the system, one arrives at a value of 2.8. Therefore, it can be assumed that the formula is based on 2.8 Ni atoms to one TCNQ molecules and resulting in an empirical formula of $Ni_{2.8}TCNQ$. The formula proposed by Jain *et al.* (see the supplementary information of reference 8) produces calculated values of the atomic % weight of: C 36.30, H 2.32, N 13.96 and Ni 27.93. Thermal gravimetric analysis showed that above 460 K there was a significant loss of mass (see Figure S1 within the supplementary information) as the sample started to decompose and this provided us with an upper temperature limit for our measurements. Powder X-ray Diffraction were conducted with a Bruker d8 diffractometer with a Cu source; the sample was measured on a glass plate, which superimposes an amorphous background onto the data, however given the amorphous nature of the sample, it is hard to untangle the background from the sample. X-ray photoelectron spectroscopy was carried out at the HarwellXPS facility. For microscopy measurements, A JEOL 2100F FEG Transmission Electron Microscope (TEM) was used which is capable of collecting Electron Energy Loss Spectroscopy (EELS) images of the samples for morphological and compositional studies. Magnetic measurements were conducted using a Quantum Design MPMS-XL with a superconducting solenoid capable of fields up to 50 kG and a temperature range of 2 to 360 K. To obtain high temperature data, the MPMS had

an oven option which allowed us to reach temperatures up to 800 K. Both zero-field cooled (ZFC) and field cooled (FC) measurements were performed in an applied field of 25 Oe. Finally, a muon spin spectroscopy (μ SR) experiment was conducted on the EMU spectrometer at the ISIS Neutron and Muon Source using closed-cycle refrigerator. A μ SR experiment involves implanted spin polarised anti-muons (μ^+) within the sample where the anti-muon, with its inherent $S = 1/2$ moment responds to any local internal fields with a ~ 2 nm radius. The μ^+ decays into a positron, with a half-life of 2.2 μ s, and this positron emitted preferentially along the direction of the μ^+ spin at the time of decay. By looking at the asymmetry of the decay of the muon spin using forward and backward detector banks one is able to probe the local static and dynamic fields resulting from both nuclear and electronic magnetism.

3. Results and discussion

It is imperative to study the chemical make-up and homogeneity of the sample to ascertain the true nature of the compound. The atomic % weights were found to be close to that obtained by Jain *et al.* [8] given the uncontrolled nature of the reaction. We note that the synthetic process is extremely unreproducible and there may be many uncontrollable factors. Our work on the reaction between $Ni(COD)_2$ and $TCNQF_4$ showed that even different solvents can have a large impact on the reaction. Therefore the deviation in % weight of our sample compared with the proposed empirical formula sample proposed by Jain *et al.* is likely to be due to the fact that the reaction does not produce a well defined crystalline sample, instead there is a substantial degree of chemical disorder. In fact, even the elemental composition shown between the two batches within the supplementary information of the original work both differed from each other and the proposed formula, where the authors had no evidence as to the form of the water or oxygen within their samples. From a powder X-ray diffraction pattern, shown within the supplementary information (see Figure S2), there is a clear bulk phase present, albeit with very broad peaks indicating a small particle size. There is also a large amorphous background, however, it is hard to unravel the background and amorphous components of the sample. The peaks correspond to bulk Ni and we have labelled the peaks with their corresponding Miller indices; there is no evidence of any other crystalline phases that might correspond to a Ni-TCNQ compound. Using the Debye-Scherrer equation and the FWHM of the (111) peak, one arrives at a particle size of approximately 4.2 nm. It should be noted this is purely an estimate, however it does tie in with the TEM data as discussed below. X-ray photoelectron spectroscopy (XPS) measurements were conducted on our samples and the results can be seen in the supplementary information (Figure S3), where the results match with that observed by Jain *et al.*, with the Ni 2p_{3/2} peak observed at 856.4 eV, which matches for that expected for Ni²⁺ ions. For additional samples, although the Ni 2p_{3/2} peak also occurs at 856.4 eV, the wider spectrum varies illustrating the inhomogeneity of the sample and the irreproducibility. XPS is a surface technique and our results likely imply that the

surface of the particles are dominated by Ni^{2+} ions likely interacting with TCNQ anions as well as other ligands such as water; however there is nothing to suggest that this surface phase is crystalline. Work by Grosvenor *et al.* [15] highlights the complexity of XPS with respect to Ni and its associated ions, where the structure of the satellite peaks is dependent on the surrounding environment of each Ni atom/ion. Given the inhomogeneity of the Ni_2TCNQ samples, one may expect a large amount of disorder and so the shape of the XPS peak can become an extremely complex problem.

Figure 1A shows a typical image of one of the Ni_2TCNQ particles; it is worth noting that there are areas of extremely different densities highlighted by the different contrasts between the dark and light regions of the particle. Therefore there appears to be some particles (dark areas) trapped within a rather low density matrix. An EELS experiment was able to show the different chemical composition of the light and dark regions of the particle. Figure 1B shows an overlay of the spatial variation of different elements. The white colour highlights where all the Ni atoms are and it is clear that these are clustered around where one sees the dark patches in Figure 1A. When looking at the distribution of nitrogen, which is present within the TCNQ molecule, this appears to be quite uniform, but is excluded within the regions that are dominated by the Ni. This is strong evidence for phase separation, where there appears to be a TCNQ based matrix encapsulating Ni particles. The oxygen distribution is restricted mainly to the edge of the particle and is not present within the Ni regions, supporting that these dark patches are purely Ni based and not an oxide. A electron diffractogram was also collected for the whole particle (see Figure 1C) and this shows that there is a phase within the sample that has a well defined structure, albeit, polycrystalline, as one can tell from the powder rings in the diffractogram with the relative spacings of the rings being consistent with a face centred cubic (fcc) structure. To further shed light on what this phase is, a high resolution TEM image (Figure 1D) was collected on the Ni regions and one can see that there is clearly structure. Within Figure 1D, we have highlighted two regions; the first clearly shows a stacking fault, where the atomic arrangement shifts at the dislocation, although it appears that this is within the same particle. The second shows that there is an atomic arrangement with a hexagonal structure, which is possibly a (111) plane of an fcc structure or the basal plane of a hexagonal close packed structure, both structures being possible for very small Ni nanoparticles. The results from the TEM measurements highlight the sample's inhomogeneity and that there is a strong phase separation between the bulk Ni nanoparticles and the organic-based matrix. The TEM results do contrast the results by XPS, where evidence for only Ni^{2+} was observed. However, the two techniques are very different; XPS probes the surface and TEM probes the bulk. Therefore one can conclude that the surface of the particles is dominated by a Ni^{2+} complex, and this likely encapsulates Ni particles within the bulk of the material. Given this ambiguity and the evidence for Ni nanoparticles, it is now worthwhile studying the magnetic properties with this in mind.

Magnetometry measurements are shown in Figure 2 and there are a few features worth noting. The first is that the low temperature behaviour shown in Figure 2A

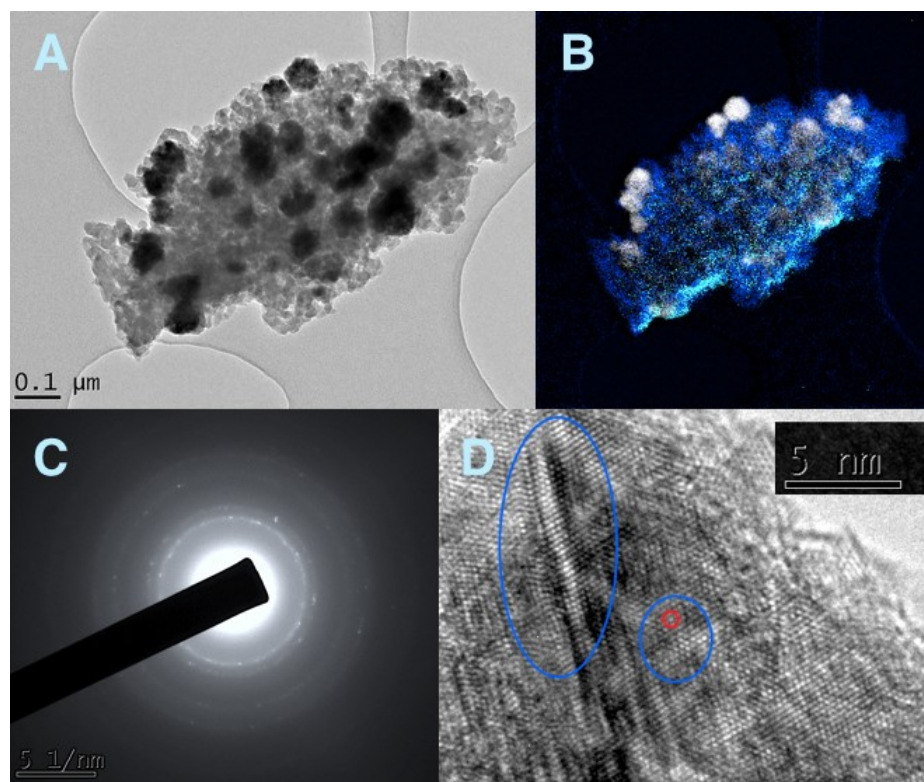


Figure 1. A collection of TEM images of a typical sample where **A:** is an image of an individual particle, **B:** is an overlay of an EELS image where white is the Ni map, dark blue is the nitrogen map and light blue is the oxygen map, **C:** is an electron diffraction pattern of the particle corresponding to FCC Ni and **D:** is a high resolution image of an area of a particle where one can see various features such as grain boundaries as well as areas with possible hexagonal packing of atoms, **the hexagonal structure associated with the Brillouin zone has been highlighted.**

is indicative of a blocking temperature of superparamagnetic particles rather than a true ferromagnetic transition. Since the data were collected in 25 Oe, one is able to see the onset of hysteresis at ~ 250 K, where the ZFC and FC curves diverge. The second point to note is the asymmetry associated with the ZFC curve in Figure 2A, where the peak is extremely broad and the asymmetry is likely to be due to a very wide distribution of particle sizes. Figure 2B shows the magnetisation at higher temperatures where the oven option was used on the magnetometer. Jain *et al.* [8] suggest that a ferromagnetic transition occurs at 480 K, however given that TGA analysis showed the sample decomposed above 460 K our measurements were limited by this. What is clear is that there is no presence of a transition within these high temperature data, instead the magnetisation gradually decreases, where the ZFC and FC curves lie, more or less, on top of each other. The data shown in Figure 2 are similar to the results obtained by Cintora-Gonzales *et al.*[16] when studying nickel nanoparticles embedded in silica gel, where the authors observed an increase of apparent blocking temperature with decreasing inter-particle separation. Such an observation has been made in many

other magnetic nanoparticulate systems (e.g. reference [17]) and is associated with the magnetic interactions between the nanoparticles [18].

Field dependent magnetisation data taken at 2 K are shown in Figure 2C. At low fields there is evidence for hysteresis as shown in Figure 2D from which we estimate a coercive field of about 400 Oe and a ‘closing’ of the hysteresis loop at fields greater than ~ 1200 Oe. At higher fields (Figure 2C) the data resemble that expected of a paramagnet as the magnetisation has not quite saturated at 50 kG. This observation is also supported by paramagnetic-like temperature dependence of the magnetisation measured at a field of 50 kG that is shown in the inset of Figure S3C that is shown within the supplementary material along with the inverse of the magnetic moment plotted as a function of T . Measurements were also made of the magnetic moment of the sample as a function of magnetic field at various fixed temperatures with data obtained at 360 K being shown in the supplementary material (Figure S3A) and, at this temperature, no magnetic hysteresis is expected as indicated by Figure 2B. The EELS and TEM data demonstrate that the synthesised Ni₂TCNQ contains a significant amount of elemental nickel in a nanoparticulate form. By assuming that these nickel nanoparticles are behaving superparamagnetically, it was possible to fit the field-dependent magnetisation data at 360 K following the example of Pisane *et al* [19], using the combination of Langevin functions weighted by a log-normal distribution function of the magnetic moments and a term which was linearly dependent upon the applied field. The fitting results are shown as the solid line in Figure S3A and this corresponded to a log-normal form of the magnetic moment distribution. Using this distribution and assuming a spherical particle, the magnetic moment distribution has been converted to a particle size distribution (see Figure S3B) and indicates the presence of wide range of nickel particle sizes (see Figure S3B). The computed nanoparticle magnetic moment distribution was used to estimate the sample’s magnetic moment at an applied field of 5 T for various temperatures, assuming that we may correct for the expected temperature dependence of the spontaneous magnetic magnetisation by adopting that of bulk nickel [20, 21]. This calculated temperature dependent magnetic moment was then subtracted from experimental data obtained at 5 T and resultant inverse magnetic moment as a function of temperature is shown in Figure S3C. It is noted that the resultant data appear to follow a Curie-Weiss law at low temperatures with a value of $\theta = -11.3(8)$ K, indicating a weakly antiferromagnetic response. A similar observation was made by Miller and Pokhodnya [9] when investigating the material produced by the synthetic route of Jain *et al.* [8] using the organic acceptor TCNE along with the solvent THF.

In addition, we have also synthesised a sample of Ni₂TCNQ using THF as the solvent. The results can be seen in Figure S2 within the supplementary information. By changing the solvent, one is able to completely change the system and its magnetic behaviour. Instead, the temperature dependence of the magnetism shows no superparamagnetic behaviour. However, plotting as χT vs. T illustrates that the situation may be more complex, where there is a splitting of the ZFC/FC curves but it is only slight, but the down turn could indicate the presence of some antiferromagnetic

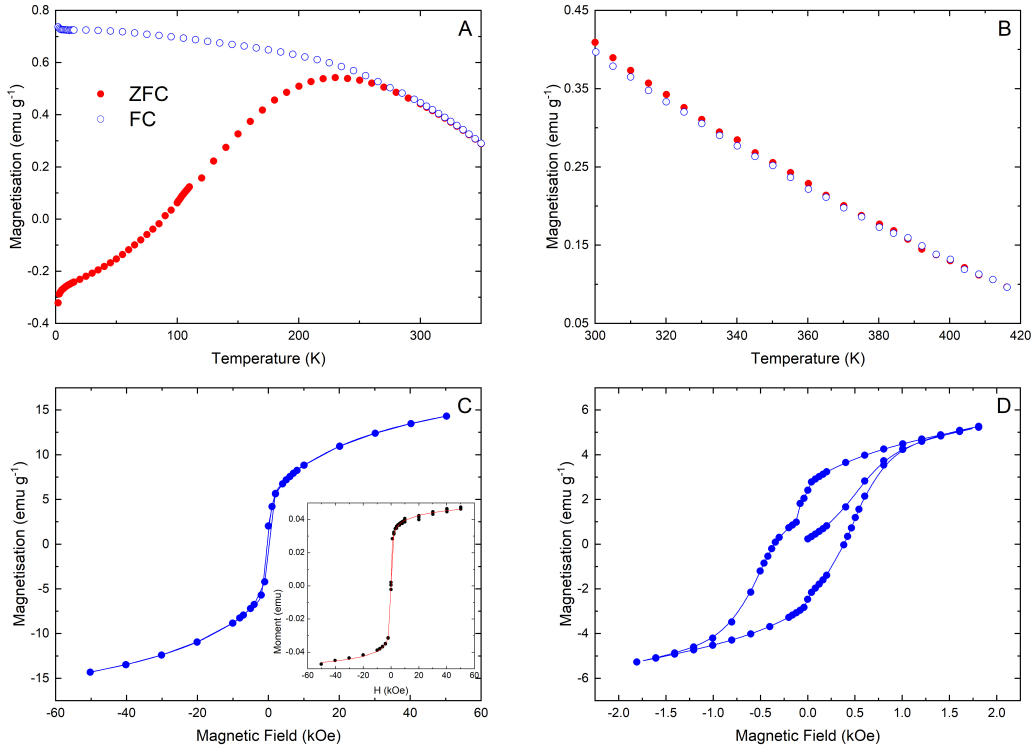


Figure 2. Magnetisation measurements on a Ni₂TCNQ sample where **A:** is the low temperature and **B:** is the high temperature part of the zero-field and field-cooled magnetisation as a function of temperature taken in an applied field of 25 Oe. **C:** Is the field dependence of the magnetisation at 2 K, the inset is the field dependence at 300 K, **D:** is the low-field hysteresis loop at 2 K showing the hysteric behaviour associated with the Ni nanoparticles.

correlations that build up as the temperature is reduced. Within previous work [8], we discuss the effect of solvent on the crystallisation process of the Ni₂TCNQF₄ sample and show that by using THF, one is able to produce a remarkably different sample where the THF is able to stabilise the formation of small Ni nanoparticles. The magnetisation *vs.* applied field data at 10 K could be fit using a summation of two Langevin functions where the number densities are $1.4(2) \times 10^{21}$ and $2.70(7) \times 10^{23} \text{ kg}^{-1}$ for both components and the respective magnetic moments are $68.1(5)$ and $6.2(1) \mu_B$. This ties together with the analysis of the Ni₂TCNQ made using the conventional route where there are two distinct particle sizes, although in this case, the THF has suppressed the formation of the larger particles, favouring the growth of smaller clusters.

In order to further study the magnetic behaviour of the Ni₂TCNQ compound one needs a probe of both local and the weak magnetism that may exist within the organic matrix material. In this case μSR is an ideal technique as it allows one to pick apart dynamic and static magnetism that arises from both nuclei and electrons on a local scale, where the muon couples via a dipolar mechanism to moments within a ~ 2 nm radius. There are also some prominent hallmarks that can clearly identify static magnetic order associated with the onset of ferromagnetism.

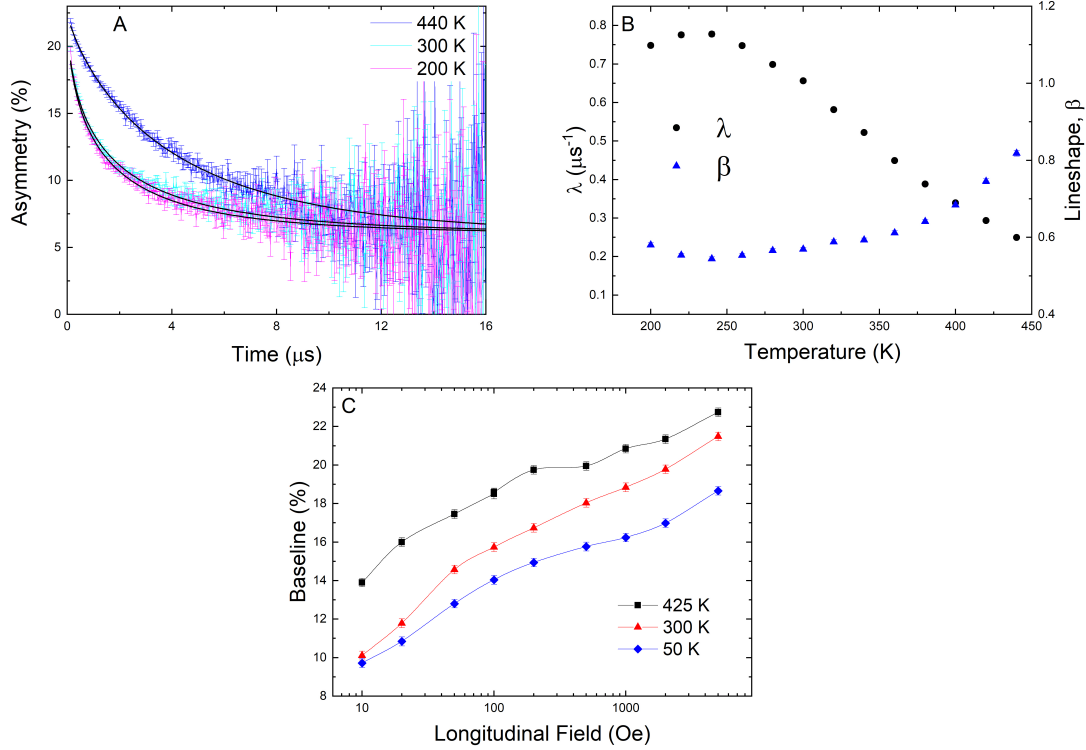


Figure 3. Muon spectroscopy data where **A:** is the raw muon spectra, **B:** The parameters from a fit to a stretched exponential showing both the muon spin relaxation rate (λ) and the line-shape (β) and **C:** is the recovery of the baseline asymmetry on application of a LF at various temperatures.

The results from the μ SR experiment are shown in Figure 3. Firstly a measurement was conducted in zero-field where compensation coils are used to screen the Earth's magnetic field. The raw muon spectra are shown in Figure 3A, where there is a strong relaxation in the asymmetry of the muon ensemble polarisation and at low temperatures the relaxation rate is much faster. One observation is that no missing fraction is observed on cooling down nor is there the onset of oscillations within the spectra that are both hallmarks of the onset of ferromagnetism. The raw data were fitted using a stretched exponential function defined as:

$$G(t) = A \exp(-\lambda t)^\beta + A_B, \quad (1)$$

where A and A_B are the relaxing and baseline asymmetry respectively, λ is the muon spin relaxation rate that is proportional to the fluctuation rate, in this case, of electronic moments, and β is the stretching exponent. The value for A was fixed at 22.5%, which is a full fraction on the EMU spectrometer. Generally, if the electronic moments are fluctuating at a single frequency such as one might expect near within the critical region of a ferromagnetic transition, then one should be able to model the data using only a single exponential. The fact that we have to employ a stretched exponential is indicating that we have a many different relaxation times and so one must stretch the exponential

function as has been seen in other nanoparticulate [22] and spin glass systems [23]. Within the temperature region of interest (200 - 450 K) there is a strong temperature dependence of both λ and β as shown in Figure 3B. The value of λ decreases as we increase the temperature up to 450 K, it should be noted that one spectra is collected over half an hour where decomposition of the sample presented a problem as the sample is sat at a high temperature for a sustained period and under vacuum. The decrease in λ reflects the increase in electronic fluctuations as the temperature is increased, this is what one would expect if going through a blocking temperature where the moments of the superparamagnetic particles begin to unfreeze going above the blocking temperature. The fact that at low temperatures β settle out a value of 0.6 gives us an indication that there is quite a wide distribution of relaxation times, where the field at the muon site is very inhomogeneous. On increasing the temperature, the value of β increases showing that the distribution of relaxation times is narrowing. **By applying a longitudinal field (LF), one can ‘decouple’ the muon from the local surrounding fields, and this can be illustrated by the increasing baseline with increasing LF. For high-purity bulk Ni, one would expect to see a step in the recovery of asymmetry when LF \sim 1400 Oe at 300 K [24]. The recovery of the baseline (Figure 3C) does not appear step-like, instead there is a very broad recovery illustrating that instead there is a range of magnetic muon environments, which is what you’d expect from an inhomogeneous system. If electronic dynamics dominate, then one cannot quench the muon spin relaxation and the baseline will not recover to the initial asymmetry.** What is clear from the data however, is that we see no evidence for a true ferromagnetic transition, instead it bears the hallmarks of a inhomogeneous magnetic system that is dominated by an unfreezing of electronic moments akin to a superparamagnet.

3.1. Conclusion

In conclusion, our work has shown that the nature of the magnetism is not due to bulk ferromagnetism. Instead, the Ni_2TCNQ sample is comprised of regions of organic material encasing Ni nanoparticles and so the system is extremely inhomogeneous, as indicated by TEM measurements. The hump in the magnetic susceptibility appears to be a blocking temperature and the muon data taken through the high temperature region shows no evidence of a bulk magnetic transition. We suggest that Jain *et al.* [8] have wrongly associated the magnetism within their samples to bulk ferromagnetism as our measurements reveal that it is dominated by the superparamagnetism of nickel nanoparticles. Therefore, although there is much promise for metal-organic based magnetism, perhaps it will not be found in materials produced by the synthetic method described in reference [8].

[1] S. J. Blundell and F. L. Pratt. 2004 *J. Phys.: Condens. Matter* **16** R771

[2] J. S. Miller. 2011 *Chem. Soc. Rev.* **40** 3266

[3] J. M. Manriquez, G. T. Yee, R. Scott McLean, A. J. Epstein and J. S. Miller. 1991 *Science* **252** 1415

[4] M. D. Harvey, T. D. Crawford and G. T. Yee. 2008 *Inorg. Chem.* **47** 5649

- [5] K. I. Pokhodnya, D. Pejakovic, A. J. Epstein and J. S. Miller. 2001 *Phys. Rev. B* **63** 174408
- [6] P.Zhou, B. G. Morin, J. S. Miller and A. J. 1993 *Phys. Rev. B* **48** 1325
- [7] B. G. Morin, P. Zhou, C. Hahm, A. J. Epstein and J. S. Miller. 1993 *J. Appl. Phys.* **73** 5648
- [8] R. Jain, K. Kabir, J. B. Gilroy, K. A. R. Mitchell, K. Wong and R. G. Hicks. 2007 *Nature* **445** 291
- [9] J. S. Miller and K. I. Pokhodnya. 2007 *J. Mater. Chem.* **17** 3585
- [10] R. Clérac, S. O’Kane, J. Cowen, X. Ouyang, R. Heintz, H. Zhao, M. J. Bazile and K. R. Dunbar. 2003 *Chem. Mater.* **15** 1840
- [11] A. Berlie, I. Terry, M. Szablewski and S. R. Giblin. 2015 *Phys. Rev. B* **92** 184431
- [12] A. Berlie, I. Terry, S. R. Giblin, T. Lancaster and M. Szablewski. 2013 *J. Appl. Phys.* **113** 17E304
- [13] A. Berlie, I. Terry and M. Szablewski. 2013 *Nanoscale* **5** 12212
- [14] A. Berlie, I. Terry and M. Szablewski. 2013 *J. Clust. Sci.* **24** 1057
- [15] A. P. Grosvenor, M. C Biesinger, R. St.C. 2006 *Surf. Sci.* **600** 1771
- [16] O. Cintora-Gonzalez, C. Estournes, M. Richard-Plouet, J.L. Guille. 2001 *Mater. Sci. Engin. C* **15** 179
- [17] E. Tronc, P. Prene, J.P. Jolivet, F. d’Orazio, F. Lucari, D. Fiorani, M. Godinho, R. Cherkaoui, M. Nogues and J.L. Dormann. *Hyp. Int.* **95** 129
- [18] J.J. Dormann, L. Bessais, D. Fiorani. 1988 *J. Phys. C* **21** 2015
- [19] K.L. Pisane, E.C. Despeaux, M.S. Seehra. 2015 *J. Magn. Magn. Mater.* **384** 148
- [20] R. Pauthenet. 1982 *J. App. Phys.* **53** 8187
- [21] J.C. Ododo. 1978 *Phys. Lett. A* **65** 444
- [22] M. H. Dehn, D. J. Arseneau, T. Buck, D. L. Cortie, D. G. Fleming, S. R. King, W. A. MacFarlane, A. M. McDonagh, R. M. L. McFadden, D. R. G. Mitchell and R. F. Kiefl. 2018 *Appl. Phys. Letts.* **112** 053105
- [23] I. A. Campbell, A. Amato, F. N. Gyax, D. Herlach, A. Schenck, R. Cywinski, and S. H. Kilcoyne. 1994 *Phys. Rev. Letts.* **72** 1291
- [24] T. Butz, J. Chappert, J.F. Dufresne, O. Hartmann, E. Karlsson, B. Lindgren, L.O. Norlin, P. Podini and A. Yaouanc. 1980 *Phys. Letts.* **75A** 321

4. Acknowledgement

The authors thank the STFC and the ISIS Neutron and Muon Source for access to muon beam time. We would also like to thank the HarwellXPS facility and in particular Dr Mark Isaacs for help with XPS measurements.